Table 1. Comparison between the dimensionless heat transfer rates at the base of the fin calculated using different models at uniform root temperature

		Exact†	Numerical‡		Modified§ [6]		Classical‖	
Bi	G_1	Q_0	Q_0	Error (%)	Q_0	Error (%)	Q_0	Error (%)
0.1	1	0.3547	0.3547	−0.0080	0.3547	−0.0080	0.3589	−1.2
0.1	5	0.5956	0.5955	−0.017	0.5970	0.23	0.6052	−1.6
1	1	1.852	1.850	0.073	1.823	−1.6	2.000	−8.0
1	5	1.806	1.799	−0.36	1.789	−0.93	2.000	−11
10	1	4.316	4.277	−0.90	3.548	−18	6.336	−47
10	5	4.091	3.952	−3.4	3.381	−17	6.325	−55

† Exact two-dimensional solution.
‡ Numerical solution of the present work.
§ Modified one-dimensional solution of ref. [6].
‖ Classical one-dimensional solution.

as is commonly adopted in the literature. For wall thickness equal to the fin thickness, it was shown that when the Bi values are less than 0.1 the root temperature is virtually uniform, but it can only be considered equal to the prescribed wall temperature for Bi less than 0.001.

It has been demonstrated that the common practice of including two-dimensional effects to account for temperature non-uniformities along the fin cross-section cannot be justified in practical situations if the root temperature is kept uniform. In situations where fin and wall have about the same thickness, only for Bi values less than 0.01 can the wall thermal resistance be neglected in calculating the heat transfer rate at the base of the fin. Usually, as walls are thicker than that, this limit has to be pushed further down. For such small values of Bi good accuracy can be achieved with the classical one-dimensional model and there is no need to employ more elaborate solutions.

REFERENCES

1. D. A. Kern and A. D. Kraus, *Extended Surface Heat Transfer*. McGraw-Hill, New York (1972).
2. R. K. Irey, Errors in the one-dimensional fin solution, *ASME J. Heat Transfer* **90,** 175–176 (1968).
3. W. Law and C. W. Tan, Errors in one-dimensional heat transfer analyses in straight and annular fins, *ASME J. Heat Transfer* **95,** 549–551 (1973).
4. L. C. Burmeister, Triangular fin performance by the heat balance integral method, *ASME J. Heat Transfer* **101,** 562–564 (1979).
5. A. D. Snider and A. D. Kraus, Recent developments in the analyses and design of extended surfaces, *ASME J. Heat Transfer* **105,** 302–306 (1983).
6. J. B. Aparecido and R. M. Cotta, Improved one-dimensional fin solutions, *Heat Transfer Engng* **11,** 49–59 (1990).
7. J. Menning and M. N. Ozisik, Coupled integral equation approach for solving melting or solidification, *Int. J. Heat Mass Transfer* **28,** 1481–1485 (1985).
8. E. M. Sparrow and D. K. Hennecke, Temperature depression at the base of a fin, *ASME J. Heat Transfer* **92,** 204–206 (1970).
9. E. M. Sparrow and L. Lee, Effects of fin base-temperature depression in a multifin array, *ASME J. Heat Transfer* **97,** 463–465 (1975).
10. D. C. Look, Jr., Two-dimensional fin with non-constant root temperature, *Int. J. Heat Mass Transfer* **32,** 977–980 (1989).
11. S. V. Patankar, *Numerical Heat Transfer and Fluid Flow*. Hemisphere, Washington, DC (1980).
12. S. V. Patankar, A numerical method for conduction in composite materials, flow in irregular geometries and conjugate heat transfer. In *Heat Transfer 1978: Proc. 6th Int. Heat Transfer Conf.*, Toronto, Vol. 3, pp. 297–302. Hemisphere, Washington, DC (1978).
13. M. N. Ozisik, *Heat Conduction*. John Wiley, New York (1980).

Int. J. Heat Mass Transfer. Vol. 36, No. 1, pp. 236–241, 1993
Printed in Great Britain

0017-9310/93 $5.00 + 0.00

Natural convection heat transfer in smooth and ribbed vertical channels

S. ACHARYA and A. MEHROTRA
Mechanical Engineering Department, Louisiana State University, Baton Rouge, LA 70803, U.S.A.

(*Received* 30 *August* 1991 *and in final form* 27 *December* 1991)

INTRODUCTION

NATURAL convection heat transfer in smooth and ribbed vertical channels is of interest in electronic cooling applications. The primary purpose of the present paper is to study natural convection heat transfer in both smooth and ribbed vertical channels, and to determine the effect of two-dimensional ribs on the smooth channel heat transfer.

As compared to the abundant literature on smooth channels (see reviews by Jaluria [1], Aihara [2] and Moffat and Ortega [3]), relatively few studies exist on natural convection in ribbed channels. Moffat and Ortega [3] and Incropera [4] have reviewed the pertinent literature. Ortega and Moffat [5, 6] have studied free convection heat transfer past a vertical adiabatic surface with three-dimensional heated protrusions. Shakerin *et al.* [7] numerically studied the effect

NOMENCLATURE

A heated surface area
b channel width
E rib height
Gr_b, Gr_b^* Grashof number, $Gr_b = g\beta(T_w - T_{in})b^3/\nu^2$, $Gr_b^* = g\beta q''_{net}b^5/L\nu^2k$
Gr_x^*, Gr_x^{**} Grashof number, $Gr_x^* = g\beta q''_{net}x^5/L\nu^2k$, $Gr_x^{**} = g\beta(T_w(x) - T_{in})x^3/\nu^2$
h heat transfer coefficient, $q_{net}/A(T_w(x) - T_{in})$
k thermal conductivity
L channel height
Nu_b, Nu_x, $\overline{Nu}_b$ Nusselt number, $Nu_b = hb/k$, $Nu_x = hx/k$, $\overline{Nu}_b = (\int_0^L Nu_b\,dx)/L$
P rib pitch
Pr Prandtl number
q, q'' power input or heat flow rate, heat flux
T temperature
x distance from the leading edge.

Greek symbols
β thermal expansion coefficient
ν kinematic viscosity.

Subscripts
b bulk, channel width
in inlet
w wall
x local.

of a protrusion on natural convection heat transfer in a differentially heated enclosure. Horton [8] studied the effect of grooves on an isothermal channel wall and Birnbreier [9] studied the effect of large barriers placed at several locations on the wall, and in both cases the Nusselt number under certain geometrical conditions were found to exceed the smooth plate values. Park and Bergles [10] found about 15% higher heat transfer coefficients with protruding heaters. Joshi *et al.* [11] experimentally studied natural convection from a vertical surface with rectangular protrusions.

The aforedescribed studies on ribbed channel heat transfer [5, 6, 8–10] appear to indicate that in the single plate limit, ribs or protrusions give Nusselt numbers higher than the corresponding smooth channel values. It is, however, misleading to make a direct comparison with heated smooth channel correlations since most of the above noted ribbed duct studies were made for heat dissipating components mounted on an *adiabatic* substrate (*not heated* as in the smooth channel studies). The numerical study of Shakerin *et al.* [7] in an enclosure revealed that ribs degraded heat transfer in the separated regions before and after the rib, and that this reduction was roughly balanced by the added surface area of the rib. It is clear that in order to definitively assess the effect of ribs on the smooth plate heat transfer, measurements have to be made in a heated channel with conducting ribs, and the Nusselt numbers compared with those from corresponding measurements without the ribs. This, therefore, is the primary objective of the present work.

EXPERIMENTS

Apparatus

The test section consists of two 15.24-cm-wide, 15.24-cm-high and 0.6-cm-thick copper plates 2.54 cm apart, each plate consisting of five copper strips separated from each other by 0.16-cm-thick non-conducting lexan strips. The lexan strips reduce longitudinal conduction between copper sections. Plexiglas extension walls are attached to the top of the copper plates in order to form a parallel plate channel. The extension walls minimize the effect of ambient disturbances on the surface heat transfer. The front and back faces of the channel are also made of plexiglas. The channel rests in a groove cut on a raised large wooden table, and is housed in a box which is packed with kao-wool insulation.

The heating circuit consists of strip heaters connected in parallel and attached to the back of each copper strip on each plate. Each strip heater is connected to a calibrated shunt and a rheostat.

Procedure

To maintain a UWT boundary condition, the rheostats are adjusted such that the maximum current passes through the bottom strip of each wall and decreases upwards. The steady state plate readings are monitored after every power adjustment and changes in the rheostat settings are made till the steady state temperatures in all the strips are within 0.2°C of each other. For the UHF boundary condition the experiments are performed so that the net heat flux per strip is the same. The differences in the net steady state heat fluxes of all the strips are reduced to within 0.5% of each other by adjusting the rheostat setting.

After completing all the experiments in a smooth channel, it is dismantled and 0.32-cm-thick, 15.2-cm-long square bronze ribs are glued to the copper strips using a thin layer of a thermally conducting bronze epoxy. Initially one rib per strip is glued, yielding a pitch to rib height ratio (P/E) of 9.6. The channel is re-assembled and the experiment is performed for identical conditions and parameters as described for the smooth channel. The pitch-to-rib height ratio is next halved by gluing a rib in between the inner-rib space (resulting in $P/E = 4.8$) and the experiments are repeated again. For all the test cases, the geometrical parameters b/L ($=0.167$) and E/b ($=0.126$) are held constant. The plate temperature measurements are made by an array of thermocouples. To permit calculation of heat losses, thermocouples are also located at other positions in the test assembly. All fluid properties are evaluated at the film temperature defined as the average of the wall and the inlet temperature.

The calculation of the Nusselt number requires the net heat flow rate q_{net} to the adjacent air stream. This term is calculated after deducting all heat losses from the power input to each strip. The losses include the lateral conduction loss through the insulation, the conduction loss through the plexiglas and the transverse loss through the strip heater respectively. These losses are determined as the product of the respective conductivities and the temperature gradients. The radiation loss from each strip to the channel top and bottom and to the opposite wall is based on the net energy exchange in an enclosure.

The maximum uncertainty in Nu_b is calculated to be $\pm 3.6\%$ and the uncertainty associated with Gr_b is found to be $\pm 2\%$.

RESULTS AND DISCUSSION

Natural convection in smooth and ribbed UWT vertical channels

For the purposes of comparing with the published data for the UWT boundary condition, experiments are first conducted without the plexiglas extension walls (as in many reported studies). The experimental results are compared in Fig. 1(a) with the experimental studies of Elenbaas [12],

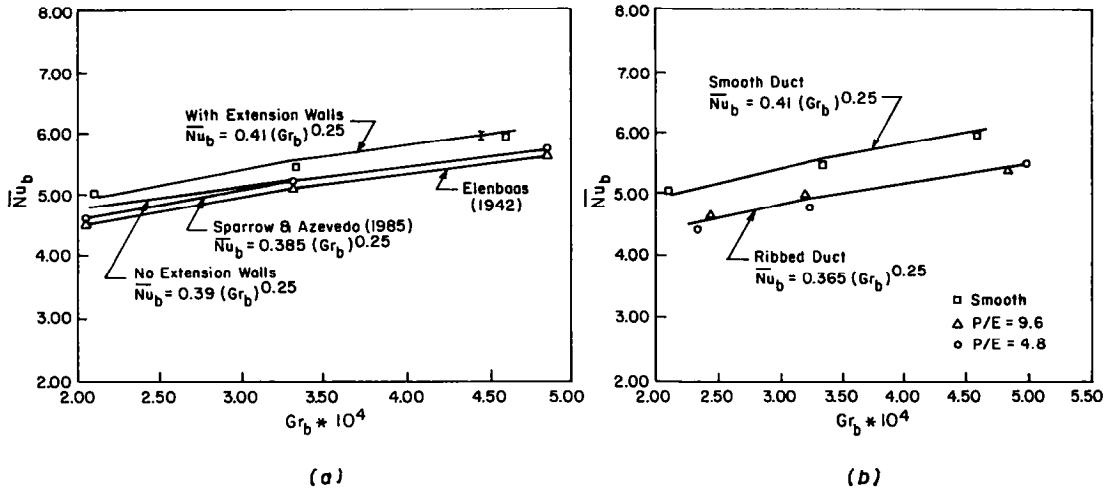

FIG. 1. Average Nusselt number, $\overline{Nu}_b$, in a UWT channel: (a) smooth channel; (b) comparison of smooth and ribbed channels (symbol I denotes error bar).

Sparrow and Azevedo [13] and the numerical study of Bodia and Osterle [14]. The maximum deviation is 5%.

The experiments are next repeated with the extension walls installed for the UWT boundary condition. The $\overline{Nu}_b$ values for this case are also plotted in Fig. 1(a), and these values are slightly higher than the corresponding values for the open channel. The $\overline{Nu}_b$ data with extension walls are correlated to within 2% by

$$\overline{Nu}_b = 0.41(Gr_b)^{0.25}. \quad (1)$$

The smooth channel has higher heat transfer rates when compared with the corresponding rates from the ribbed geometries (Fig. 1(b)). This is an important observation since many designs for electronic cooling systems are based on the smooth plate correlations. In the earlier discussion of the literature, many studies have reported higher heat transfer values for the adiabatic channel with heated protrusions compared to the smooth heated vertical channel. The measurements of this study clearly indicate that, with ribs, the surface heat transfer decreases by about 10–13%. The probable reason for the lower heat transfer from the ribbed surfaces is the dead region created in the near-rib space. The numerical predictions of Shakerin *et al.* [7] in a rectangular enclosure revealed recirculation regions before and after the rib and surface heat transfer in these recirculation regions is lower than the corresponding smooth plate values. The existence of these trapped recirculation regions for the $P/E = 4.8$ case is also confirmed by the recent flow visualization pictures of Joshi *et al.* [11].

The $\overline{Nu}_b$ data for the two ribbed duct geometries are correlated by the expression:

$$\overline{Nu}_b = 0.365(Gr_b)^{0.25} \quad (2)$$

with a maximum deviation of less than 2.9%. When the data are correlated separately the leading coefficient is 0.37 for $P/E = 9.6$ and 0.36 for $P/E = 4.8$; the Gr_b exponent is the same. Since the $\overline{Nu}_b$ values for the two P/E cases differ by an amount that is of the order of the experimental uncertainty, a single correlation for the two cases, given by equation (2), is more appropriate.

In Fig. 2, local Nusselt numbers are plotted and it is observed that Nu_b decreases downstream of the leading edge

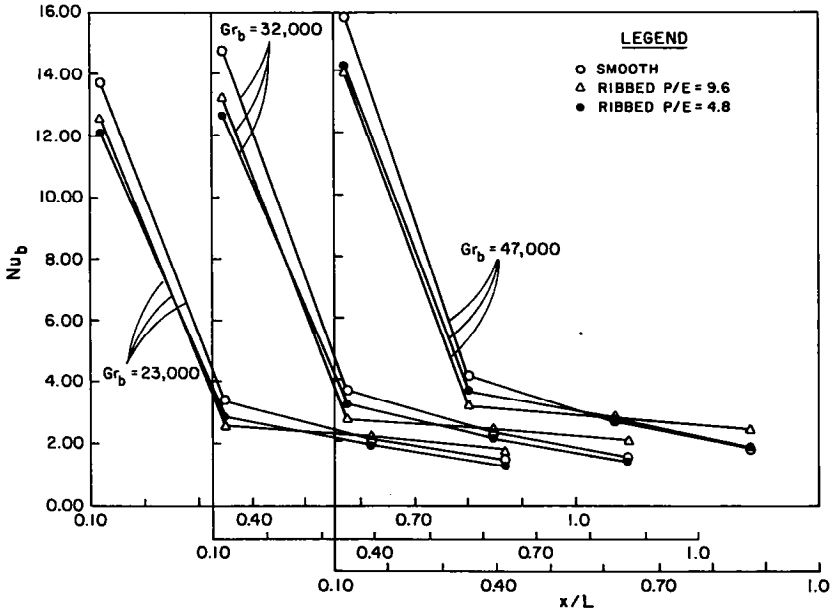

FIG. 2. Local Nusselt number, Nu_b, in a UWT channel.

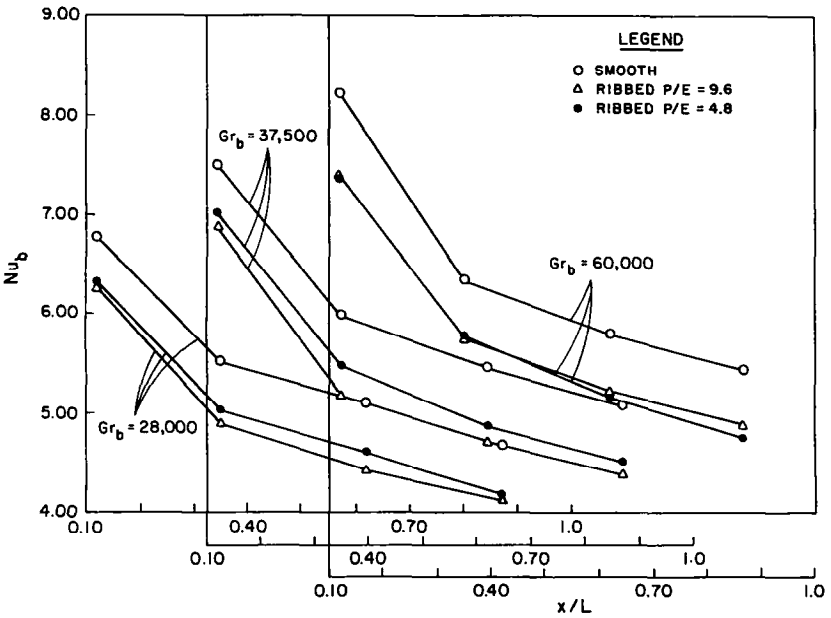

FIG. 3. Local Nusselt number, Nu_b, in a UHF channel.

for both the smooth and the ribbed geometries. It should be noted that Nu_b or Nu_x profiles do not depict the true local behavior since these are strip-averaged values that have been joined by straight lines. As expected, the Nu_b values increase with an increase in Grashof number. The $P/E = 9.6$ case appears to asymptote more rapidly than the smooth and $P/E = 4.8$ cases.

Natural convection in smooth and ribbed UHF vertical channels

The temperature difference downstream of the leading edge non-dimensionalized by the difference at the channel exit is correlated as:

$$\frac{T_w(x) - T_{in}}{T_w(L) - T_{in}} = \left(\frac{x}{L}\right)^{0.20} \tag{3}$$

with a maximum r.m.s. error of 2.8%. This correlation is the same as the one proposed by Wirtz and Stutzman [15] for a vertical channel and seems to indicate that the boundary layer flow on each plate of the channel is closer to the single plate behavior than the fully developed channel behavior. The Nusselt number value at the channel exit, Nu_L, which is inversely proportional to the corresponding plate temperature, expectedly compares well with that of Wirtz and Stutzman [15].

Local Nu_x values, based on the distance downstream of the leading edge, are correlated to within 1.3% by

$$Nu_x = 0.64(Gr_x^* Pr)^{0.2} \tag{4}$$

and this compares well with Vliet's [16] correlation for a vertical plate given by:

$$Nu_x = 0.6(Gr_x^* Pr)^{0.2}. \tag{5}$$

As noted above, this suggests a very small effect of the opposite wall.

A comparison of the strip-averaged Nu_b is made for the three geometries at varying Gr_b^* values in Fig. 3. The smooth duct yields a greater heat transfer rate at all values of Grashof number when compared with the heat transfer rates for the ribbed geometries. As discussed in the previous section, the probable reason for the reduced heat transfer from the ribbed surfaces is the dead region created in the near-rib space.

On comparing the two ribbed geometries, $P/E = 9.6$ and 4.8, the lower pitch geometry yields higher Nu_b values at Gr_b^* values of 28 000 and 37 500, with the maximum deviation generally occurring at the second strip. With the increase in Gr_b^* to 60 000, the two curves are very close to each other, with the Nu_b value for $P/E = 4.8$ dropping below the $P/E = 9.6$ value after the third rib. To explain this behavior, detailed flow and temperature measurements are needed. However, one can speculate on possible reasons. Ribs can lead to two counteracting effects. The first, and already mentioned as the possible reason for Nu values in a ribbed channel being lower than in a smooth channel, is the formation of a separation region near the rib which inhibits the heat transfer. The second effect, and one which promotes heat transfer, is that the ribs serve to increase the heat transfer area. The second effect may explain why in many of the cases the Nu_b values for $P/E = 4.8$ are larger than the values for $P/E = 9.6$ (there are twice as many ribs with $P/E = 4.8$ as with $P/E = 9.6$). However, with increasing Grashof number, the first effect appears to become increasingly more important since for the highest Grashof number studied, the Nu_b values for the case with a smaller number of ribs ($P/E = 9.6$) attains higher trailing edge values than for $P/E = 4.8$.

Local values of Nu_x are plotted against Gr_x^* for the ribbed cases in Fig. 4(a). The correlation for the ribbed duct ($P/E = 9.6$ and 4.8) can be expressed as

$$Nu_x = 0.555(Gr_x^* Pr)^{0.2} \tag{6}$$

with an r.m.s. error of less than 4%. The correlated values for the ribbed duct are generally 15% lower than the smooth duct values (equation (4)). The exponent in the ribbed duct correlations also match those of Vliet's [16] correlation for a single UHF vertical plate. This indicates that for the ribbed channel also, there is very little interaction between the symmetrically heated channel walls.

The results of this study for the ribbed geometries are also correlated (with an r.m.s. error of less than 5%), as in Ortega and Moffat [6], by defining a local Gr_x^{**} based on a local wall to inlet temperature difference:

$$Nu_x = 0.535(Gr_x^{**} Pr)^{0.25} \text{ (smooth)}$$
$$Nu_x = 0.48(Gr_x^{**} Pr)^{0.25} \ (P/E = 9.6, 4.8). \tag{7}$$

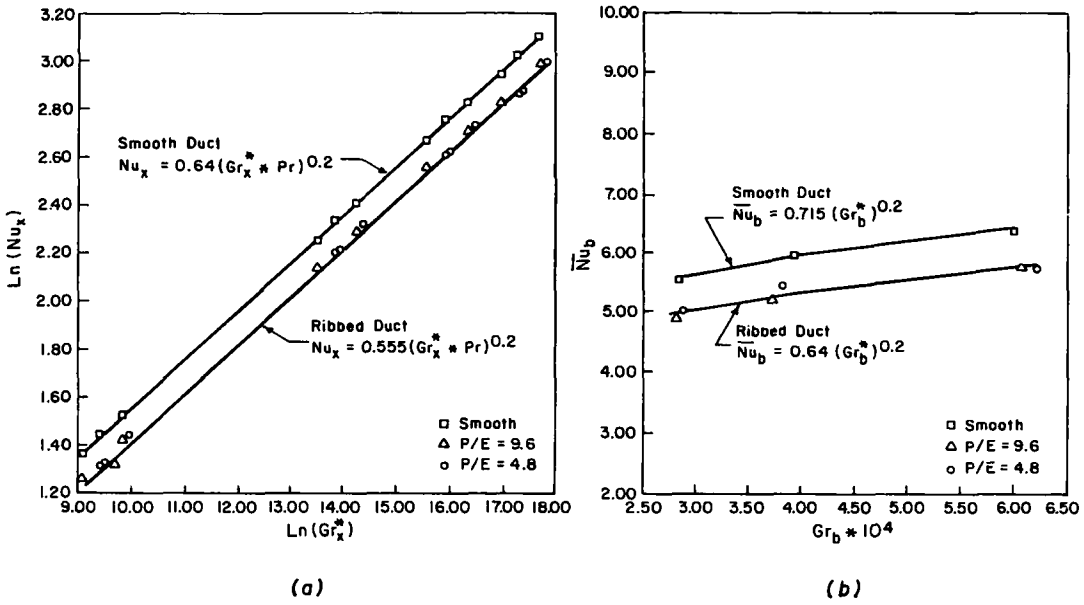

FIG. 4. (a) Local Nusselt number, Nu_x, in a UHF channel. (b) Average Nusselt number, $\overline{Nu}_b$, in a UHF channel.

Moffat and Ortega [3], for three-dimensional ribs mounted on an adiabatic substrate, found Nu_x to vary as $(Gr_x^{**})^{0.33}$, indicating higher heat transfer from the ribbed surface compared to a smooth surface. In the present study, $Nu_x \sim (Gr_x^{**})^{0.25}$ for both the ribbed and smooth plates, and the ribbed plate heat transfer is smaller than the smooth plate. The higher exponent in Ortega and Moffat's work is probably due to the three-dimensional ribs, higher Gr_x^{**} values, and quite different thermal conditions along the channel walls. As noted earlier, care should be taken in comparing ribbed duct correlations with smooth duct correlations in order to assess the effect of ribs on heat transfer.

The average Nusselt number $\overline{Nu}_b$ for the smooth UHF duct (Fig. 4(b)) is correlated to within 1.45% by

$$\overline{Nu}_b = 0.715(Gr_b^*)^{0.2} \quad (8)$$

whereas the ribbed duct data is correlated by the expression:

$$\overline{Nu}_b = 0.64(Gr_b^*)^{0.2} \quad (9)$$

with a maximum deviation of 2.68%.

CONCLUDING REMARKS

An experimental study has been made of natural convection heat transfer in smooth and ribbed UWT and UHF vertical channels. In both the UWT and UHF cases studied, the ribbed duct heat transfer is lower than the smooth duct heat transfer. The UWT data are correlated by $\overline{Nu}_b = K Gr_b^{0.25}$, with $K = 0.41$ for the smooth duct and $K = 0.365$ for the ribbed ducts ($P/E = 9.6$ and 4.8). The UHF data are correlated, similarly, by $\overline{Nu}_b = K(Gr_b^*)^{0.2}$, with $K = 0.715$ for the smooth channel and 0.64 for the ribbed cases. The Grashof number exponents indicate that for both the smooth and ribbed channels the single plate behavior is valid.

The measurements clearly establish the reduction in natural convection heat transfer due to the ribs, and indicate that in comparing ribbed duct data with smooth duct data, care should be taken to ensure that the geometry and thermal conditions are equivalent.

REFERENCES

1. Y. Jaluria, Natural convection cooling of electronic equipment. In *Natural Convection, Fundamentals and Applications* (Edited by S. Kakac, W. Aung and R. Viskanta). Hemisphere, New York (1985).
2. T. Aihara, Effects of inlet boundary-conditions on numerical solutions of free convection between vertical parallel plates, Report Number 258 of the Institute of High Speed Mechanics, Tohoku University, Japan, pp. 1–28 (1972).
3. R. J. Moffat and A. Ortega, Direct air-cooling of electronic components. In *Advances in Thermal Modelling of Electronic Components and Systems* (Edited by A. Bar Cohen and A. Kraus), Vol. 1, pp. 129–265. Hemisphere, New York (1988).
4. F. Incropera, Convection heat transfer in electronic equipment cooling, *J. Heat Transfer* **110**, 1097–1111 (1988).
5. A. Ortega and R. J. Moffat, Heat transfer from an array of simulated electronic components: experimental results for free convection with and without a shrouding wall, *ASME HTD* **48**, 5–15 (1985).
6. A. Ortega and R. J. Moffat, Buoyancy induced convection in a non-uniformly heated array of cubical elements on a vertical channel wall, *Heat Transfer in Electronic Equipment, ASME HTD* **57**, 123–134 (1986).
7. S. Shakerin, M. Bohn and R. I. Loehrke, Natural convection in an enclosure with discrete roughness elements on a vertical heated wall, *Proc. 8th Int. Heat Transfer Conf.*, San Francisco, Vol. 4, pp. 1519–1525 (1986).
8. S. F. Horton, Natural convection from parallel plates with grooved surfaces, M.S. Thesis, Department of Mechanical Engineering, MIT, Boston (1981).
9. H. Birnbreier, Experimental investigation on the temperature rise of printed circuit boards in open cabinets with natural ventilation, *ASME HTD* **20**, 19–23 (1981).
10. K. A. Park and A. E. Bergles, Natural convection heat transfer characteristics of simulated microelectronic chips, *J. Heat Transfer* **100**, 243–253 (1987).
11. Y. Joshi, T. Wilson and S. J. Hazard, An array of heated

protrusions on a vertical surface in water, *J. Electronic Packaging* **111**, 121–128 (1989).
12. W. Elenbaas, Heat dissipation of parallel plates by free convection, *Physica* **9**, 1–28 (1942).
13. E. M. Sparrow and L. F. A. Azevedo, Vertical-channel natural convection spanning between the fully developed limit and the single-plate boundary-layer limit, *J. Heat Transfer* **28**, 1847–1857 (1985).
14. J. R. Bodia and J. F. Osterle, The development of free convection between heated vertical plates, *J. Heat Transfer* **84**, 40–44 (1961).
15. R. A. Wirtz and R. J. Stutzman, Experiments on free convection between vertical plates with symmetric heating, *J. Heat Transfer* **104**, 501–507 (1982).
16. G. C. Vliet, Natural convection local heat transfer on constant heat flux inclined surfaces, *Int. J. Heat Mass Transfer* **18**, 511–517 (1969).

Int. J. Heat Mass Transfer. Vol. 36, No. 1, pp. 241–243, 1993
Printed in Great Britain

0017-9310/93 $5.00 + 0.00

The combined effects of fog formation and Stefan flow on nickel and iron evaporation into helium

H. J. H. BROUWERS†

Akzo Research Laboratories Arnhem, Fibers Division, Department of Mechanical Engineering, Velperweg 76, 6824 BM Arnhem, The Netherlands

(*Received* 11 *November* 1991)

INTRODUCTION

ONE FIELD of problems involving the combined effects of Stefan flow and fog formation is the evaporation of molten metals into much colder gases. The enhancement of induction-heated iron/nickel alloys evaporation into stagnant helium by fog formation has been described theoretically by Turkdogan [1], Rosner [2] and Hills and Szekely [3, 4], and investigated experimentally by Turkdogan and Mills [5]. In some experiments Toop [6] also found that metal evaporation occurs at rates considerably higher than those predicted by conventional mass transfer correlations.

The former two investigators treated supersaturation in the gas in terms of a 'critical supersaturation model' (CSM). In both papers the assumption was made that the temperature field in the stagnant film is undisturbed by fog formation and therefore remains a linear function of the coordinate. This representation of the process is allowed only in cases where the vapour is extremely dilute.

On the basis of a combined analysis of the energy and diffusion equations, coupled with the basic saturation condition (thus excluding supersaturation), Hills and Szekely [4] obtained good agreement with the experimental data of Turkdogan and Mills [5]. In all the discussed analyses of iron/nickel alloys evaporation, however, Stefan flow in the considered transferring film was not taken into account, despite the fact that Rosner [2] and Hills and Szekely [4] mentioned that Stefan flow cannot be neglected for temperatures above 2000°C.

To provide a rather more rigorous representation of the process, the procedure suggested by Brouwers [7] for the combined effects of Stefan flow and the condensation mechanism is applied in this note. First, the existence and magnitude of a fog layer is determined. Next, the mass transfer correction factor that reckons with both fog formation and Stefan flow is applied to the process. This correction factor followed from the asymptotic approximation solution of the energy and diffusion equations, coupled by the saturation condition, of a stagnant film including fog formation and Stefan flow (referred to as 'induced velocity'). Furthermore, the compound correction factor of Brouwers [8] is also employed to assess said effects. This correction factor originates from a multiplication of the classical film model correction factor for Stefan flow by the fog film model correction factor for fog only.

† Present address: Department of Civil Engineering, Twente University, P.O. Box 217, 7500 AE Enschede, The Netherlands.

FORMULATION

A stagnant helium film next to an iron and or nickel evaporating wall is considered. At the liquid surface ($y = 0$) the iron/nickel (or vapour) mass fraction is c_i and the temperature t_i. At a distance δ_c the bulk vapour mass fraction c_b is attained, and at a distance δ_t the bulk temperature t_b. As both the vapour pressures and molecular masses of iron and nickel are very similar, the approximation of Hills and Szekely [4] is adopted by considering the evaporation of pure nickel only.

The first step is to examine whether fog is formed in part or all of the film. To this end, the slope condition of Brouwers [7] is utilized to verify if supersaturation takes place

$$\left.\frac{\mathrm{d}F}{\mathrm{d}t}\right|_{t_i} > Le_v \frac{c_i - 1}{t_b - t_i}\left[\exp\left\{\frac{\delta_t}{Le_v \delta_c}\ln\left(\frac{1-c_b}{1-c_i}\right)\right\} - 1\right] \quad (1)$$

where interface vapour fraction $c_i = F(t_i)$. The saturation line $F(t)$ follows from the thermally perfect gas law and Gibbs–Dalton's law

$$F(t) = \frac{M_v P_v(t)}{M_v P_v(t) + M_n (P_{tot} - P_v(t))}. \quad (2)$$

The total absolute pressure P_{tot} of the nickel–helium mixture considered amounts to 1 atm (= 1.01325 bar) and the bulk properties concerned are: $t_b = 77$°C, $c_b = 0$. The molecular mass M_v of nickel and M_n of helium are 58.71 and 4.00 kg kmol^{-1}, respectively. The liquid saturation pressure of nickel, $\ln(P_v/[\text{bar}]) = 32.41 - 51\,578/T/[\text{K}] - 2.01 \ln(T/[\text{K}])$, taken from Smithells [9], is applicable since $t_i \geqslant 1500$°C, which is well above the melting point of nickel ($\cong 1455$°C).

In view of the fact that Le is close to unity (typically $Le = 2.2$, see Rosner [2], this value is used throughout this note) and the absence of externally imposed flow, the approximation $\delta_t = \delta_c$ is applicable. The specific heat of the mixture follows from the expression for perfect monatomic gases:

$$c_p = \frac{5R}{2M} \quad (3)$$

where R is the universal gas constant, $R = 8316.94$ J kmol^{-1} K^{-1}. The mean molecular mass M is evaluated with the help of the arithmetic mean of the mole fractions of nickel and helium at the interface and bulk. The specific heat $c_{p,v}$ of nickel readily follows from equation (3) when $M = M_v$ is substituted. With Le, c_p and $c_{p,v}$ determined, Le_v is now specified. For the entire t_i range examined, 1500°C $\leqslant t_i$